

Article

Low-Temperature Methane Partial Oxidation over Pd Supported on CeO₂: Effect of the Preparation Method and Precursors

Shiva Fazlikeshteli, Xavier Vendrell *  and Jordi Llorca * 

Institute of Energy Technologies, Department of Chemical Engineering and Barcelona Research Center in Multiscale Science and Engineering, Universitat Politècnica de Catalunya, EEBE, Eduard Maristany 10-14, 08019 Barcelona, Spain; shiva.fazlikeshteli@upc.edu

* Correspondence: xavier.vendrell.villafuela@upc.edu (X.V.); jordi.llerca@upc.edu (J.L.)

Abstract: The catalytic production of syngas by the partial oxidation of methane (POM) was investigated over Pd supported on ceria (0.5–2 Pd wt.%) prepared by incipient wetness impregnation and by mechanochemical methods. The performance of the Pd/CeO₂ catalyst prepared by milling CeO₂ and Pd acetate was superior to that prepared by milling CeO₂ and Pd nitrate and to Pd/CeO₂ prepared by impregnation from Pd acetate. The best catalytic activity of the Pd/CeO₂ catalyst prepared from CeO₂ and Pd acetate was obtained by milling at 50 Hz for 5 min. Two-step combustion and reforming reaction mechanism were identified. Remarkably, methane conversion increased progressively with Pd loading for the catalysts prepared by incipient wetness impregnation, whereas low metal loading showed better conversion of methane for the catalysts prepared by ball milling using Pd acetate. This was explained in terms of an impressive dispersion of Pd species with a strong interaction with the surface of ceria, as deduced from transmission electron microscopy, Raman spectroscopy and X-ray photoelectron spectroscopy characterization, which revealed a large quantity of highly oxidized species at the surface.



Citation: Fazlikeshteli, S.; Vendrell, X.; Llorca, J. Low-Temperature Methane Partial Oxidation over Pd Supported on CeO₂: Effect of the Preparation Method and Precursors. *Reactions* **2021**, *2*, 30–42. <https://doi.org/10.3390/reactions2010004>

Received: 20 January 2021

Accepted: 11 February 2021

Published: 17 February 2021

Publisher's Note: MDPI stays neutral with regard to jurisdictional claims in published maps and institutional affiliations.



Copyright: © 2021 by the authors. Licensee MDPI, Basel, Switzerland. This article is an open access article distributed under the terms and conditions of the Creative Commons Attribution (CC BY) license (<https://creativecommons.org/licenses/by/4.0/>).

Keywords: methane partial oxidation; syngas; palladium; ceria catalysts; mechanochemistry

1. Introduction

Converting methane to syngas represents a well-known method for natural gas valorization and upgrade into valuable chemicals as well as a route for the production of hydrogen for energy applications [1–5]. This can be accomplished by catalytic partial oxidation (POM), $\text{CH}_4 + \frac{1}{2}\text{O}_2 \rightarrow \text{CO} + 2\text{H}_2$ ($\Delta H_{298} = -36 \text{ kJ mol}^{-1}$), with carbon soot, CO₂ and H₂O being the main by-products. There is currently no consensus on the mechanism of the POM reaction, and two different mechanisms have been proposed. In the first one, often referred to as the direct partial oxidation, synthesis gas is a primary product of the reaction, which proceeds from direct methane dissociation on the catalyst surface followed by oxidation of adsorbed oxygen [6]. The second mechanism involves two steps. First, methane reacts with oxygen to yield CO₂ and H₂O, $\text{CH}_4 + 2\text{O}_2 \rightarrow \text{CO}_2 + 2\text{H}_2\text{O}$ ($\Delta H_{298} = -803 \text{ kJ mol}^{-1}$). Second, the unreacted methane is reformed with the steam and CO₂ produced in the first step to yield syngas, $\text{CH}_4 + \text{H}_2\text{O} \rightleftharpoons \text{CO} + 3\text{H}_2$ ($\Delta H_{298} = +206 \text{ kJ mol}^{-1}$) and $\text{CH}_4 + \text{CO}_2 \rightleftharpoons 2\text{CO} + 2\text{H}_2$ ($\Delta H_{298} = +247 \text{ kJ mol}^{-1}$), respectively [7,8]. In this case, although the overall reaction remains exothermic, there are two steps involved, one being exothermic (methane oxidation) and the other endothermic (methane steam reforming and dry reforming). In addition, the water gas-shift equilibrium is always present, $\text{CO}_2 + \text{H}_2 \rightleftharpoons \text{CO} + \text{H}_2\text{O}$ ($\Delta H_{298} = -41 \text{ kJ mol}^{-1}$).

Numerous catalyst formulations have been tested so far for POM, with those based on Ni, Co and Fe (and Cu to a lesser extent), transition metal carbides and noble metals (Rh, Pt and Ru, and to a lesser extent Pd and Ir), and combinations thereof, being the most successful [9–15]. Nickel-based catalysts have been widely used because they are cheap and very

active, but they are prone to carbon deposition, which results in catalyst deactivation. Palladium is one of the most effective noble metal catalysts for methane activation, particularly when it is supported on supports with redox properties. In particular, the metal-support interaction established between Pd and cerium dioxide has shown excellent properties for the activation of C-H bonds in the methane molecule, which originates from the oxygen storage-release properties of ceria and the stabilization of oxidized Pd species [16]. In addition, ceria facilitates the oxidation and removal of any soot deposited [17–19].

As commonly occurs in catalysis, the intricate properties of the metal-support interaction depend on the method used for the preparation of the catalyst. In recent years, it has been demonstrated that different architectures of the Pd-CeO₂ interface are obtained by using conventional impregnation or solution combustion synthesis or mechanochemical methods, which strongly determine the performance of the resulting Pd/CeO₂ catalysts in the total oxidation of methane [20–23]. In particular, advanced operando characterization has recently shown that catalysts prepared by mechanical milling are clearly superior because they contain very stable palladium species [24]. In this work, we study Pd/CeO₂ catalysts prepared by incipient wetness impregnation and by dry ball milling using Pd nitrate and Pd acetate for low-temperature POM.

2. Materials and Methods

2.1. Preparation of Catalysts

Cerium dioxide was prepared by adding NH₄OH to an aqueous solution of Ce(NO₃)₃·6H₂O until pH~9.5. The mixture was aged for 24 h and the resulting precipitate was dried and calcined at 650 °C for 4 hours (5 °C min⁻¹). Palladium nitrate and palladium acetate were used as Pd precursors and the Pd loading of the catalysts was varied between 0.5 and 2 wt.%. For the ball milled samples (labeled as BM), the Pd precursor was mixed directly with cerium dioxide in a zirconium oxide vessel (1 g of sample and 1 zirconium oxide ball of 15 mm diameter) using a Fritsch Pulverisette 23 (Idar-Oberstein, Germany) mini-mill apparatus. The effect of ball mill energy was explored in the range 15–50 Hz, and the effect of milling time was studied in the range 5–20 min. Samples prepared by conventional incipient wetness impregnation (labeled as IWI) from palladium acetate or palladium nitrate were calcined at 650 °C for 4 h (5 °C min⁻¹). To check for ball milling effects on the ceria support, additional samples were prepared by incipient wetness impregnation on previously ball milled CeO₂ at 50 Hz for 10 min. No further treatments were performed on the calcined samples prior to the catalysts tests.

2.2. Catalyst Characterization

X-ray diffraction (XRD) was performed using a Siemens D5000 (Munich, Germany) diffractometer equipped with a Cu K α radiation source (45 kV, 35 mA) in Bragg-Brentano geometry using steps of 0.02° at 1 s per step. The crystallite size was calculated with the Debye-Scherrer formula. Raman spectroscopy was performed using a Renishaw inVia Qontor confocal Raman microscope (Gloucestershire, UK) equipped with a 532.1 nm laser with a nominal 100 mW output power directed through a especially adapted Leica DM2700 M microscope (x50 magnification) (Wetzlar, Germany). X-ray photoelectron spectroscopy (XPS) was performed with a SPECS system (Berlin, Germany) equipped with a XR50 source operating at 250 W and a Phoibos 150 MCD-9 detector. The pass energy of the high-resolution spectra was set at 0.1 eV. Binding energy (BE) values were referred to the Ce⁴⁺ 3d_{5/2} peak at 916.9 eV. High-resolution transmission electron microscopy (HRTEM) was performed with a FEI TECNAI F20 S/TEM instrument (Hillsboro OR, USA) operated at 200 kV and equipped with a field emission electron source.

2.3. Catalytic Tests

The partial oxidation of methane (POM) was carried out at atmospheric pressure in a quartz reactor. The catalyst (0.1 g) was diluted with SiC to obtain a fixed bed volume of 0.5 cm³. Temperature-dependent catalytic activity measurements were carried out between

200 and 600 °C at steps of 50 °C (ca. 40 min at each temperature) using a total gas flow of 100 mL min⁻¹ (GHSV = 1.2 × 10⁴ h⁻¹) and a CH₄:air:N₂ ratio of 4:11:85 on a molar basis (F/W = 60 L h⁻¹ g⁻¹). Products were analyzed on-line by gas chromatography with a Varian CP-4900 instrument (Palo Alto CA, USA) equipped with Molecular Sieve of 5 Å, Plot U and Stabilwax columns for a complete analysis of products. Methane conversion (x_{CH_4}) is defined by Equation (1), where F_{inCH_4} and F_{outCH_4} are the inlet and outlet molar flow of methane, respectively.

$$x_{CH_4} = \frac{F_{inCH_4} - F_{outCH_4}}{F_{inCH_4}} \times 100 \quad (1)$$

Selectivity of hydrogen (S_{H_2}) and carbon monoxide (S_{CO}) are calculated using Equations (2) and (3), respectively.

$$S_{H_2} = \frac{\text{moles of } H_2 \text{ produced}}{2 \times \text{moles of } CH_4 \text{ consumed}} \times 100 \quad (2)$$

$$S_{CO} = \frac{\text{moles of } CO \text{ produced}}{\text{moles of } CH_4 \text{ consumed}} \times 100 \quad (3)$$

3. Results and Discussion

3.1. Characterization

The microstructure of the catalysts was studied by high-resolution transmission electron microscopy (HRTEM) and energy-dispersive X-ray analysis (EDX). Figure 1a shows a representative image of the sample prepared by milling CeO₂ and Pd acetate (50 Hz, 10 min, 1 wt.% Pd). As reported in a previous work [24], the mechanochemical synthesis of Pd/CeO₂ using Pd acetate creates an amorphous layer on the ceria crystallites. This shell exhibits an average thickness of about 2–3 nm. The EDX analysis of the amorphous layer (inset in Figure 1a) shows the simultaneous occurrence of Ce, Pd and O (the Cu signal originates from the TEM grid), which indicates that this layer is constituted by a Pd-O-Ce phase. Figure 1b corresponds to the sample prepared by milling CeO₂ and Pd nitrate (also 50 Hz, 10 min, 1 wt.% Pd). The substitution of Pd acetate by Pd nitrate in the mechanochemical preparation method originates a very different microstructure. Instead of an amorphous Pd-O-Ce shell, the sample contains subnanometric Pd entities, which are well dispersed on the ceria support. Some of these subnanometric Pd entities are enclosed in a red circle in Figure 1b. Figure 1c shows the microstructure of the sample prepared by incipient wetness impregnation with Pd acetate (1 wt.% Pd). In contrast with the catalysts prepared by mechanochemistry, the incipient wetness impregnated sample using Pd acetate shows the occurrence of well-defined Pd nanoparticles, which measure about 3–4 nm. Figure 1c corresponds to the sample prepared by incipient wetness impregnation with Pd nitrate (1 wt.% Pd). Individual Pd nanoparticles are also encountered, but the use of Pd nitrate as precursor results in smaller Pd nanoparticles, which measure about 1–2 nm.

The X-ray diffraction (XRD) patterns and Raman spectra recorded for the samples studied by TEM are shown in Figure 2. For all samples, the only peaks detected by XRD were those corresponding to the CeO₂ support. No peaks associated with Pd phases were present due to the low Pd loading (1 wt.%) and no variation of the lattice parameter of CeO₂ was detected, excluding the possibility of Pd incorporation in the ceria structure. The size of the ceria crystallites decreased as a result of ball milling, from about 35 nm down to 31.6 nm after ball milling for 5 min at 50 Hz and 26.7 nm after ball milling for 10 min at 50 Hz. The Raman spectra were dominated by the characteristic F_{2g} band of the ceria lattice structure at about 463 cm⁻¹ [25] (the band at ca. 718 cm⁻¹ was due to the sample holder). The defect-induced vibrational mode at about 595 cm⁻¹ (D band) was nearly absent in all samples, which means that the incorporation of Pd did not result in the formation of lattice defects in the ceria structure, such as oxygen vacancies [26]. It is worth noting that the main F_{2g} peak of ceria shifted slightly to lower wavelengths

(460 cm^{-1}) after incorporation of Pd with the ball milling method with respect to the CeO_2 support, whereas it appeared at the same wavelength for the samples prepared by impregnation. Taking into account that the F_{2g} band of ceria did not shift after ball milling in the absence of Pd, this is likely caused by an enhanced Pd–support interaction in the samples prepared by mechanochemistry [27]. The Raman spectrum of the sample prepared by milling CeO_2 and Pd acetate showed a weak band at 945 cm^{-1} , which corresponds to the (C- CH_3) mode of the acetate group, and the Raman spectrum of the sample prepared by milling CeO_2 and Pd nitrate showed a weak band at 1046 cm^{-1} , which corresponds to the symmetric ν_1 stretching mode of the nitrate anion [28]. These bands were absent in the catalysts prepared by impregnation, because the acetate and nitrate residues disappeared following the calcination treatment performed at $650\text{ }^\circ\text{C}$ (see Section 2.1). Finally, the Raman spectrum of the catalyst prepared by impregnating CeO_2 with Pd nitrate exhibited a band at 650 cm^{-1} , which is ascribed to the B_{1g} mode of PdO and suggests that this sample contains well-defined PdO nanoparticles [29].

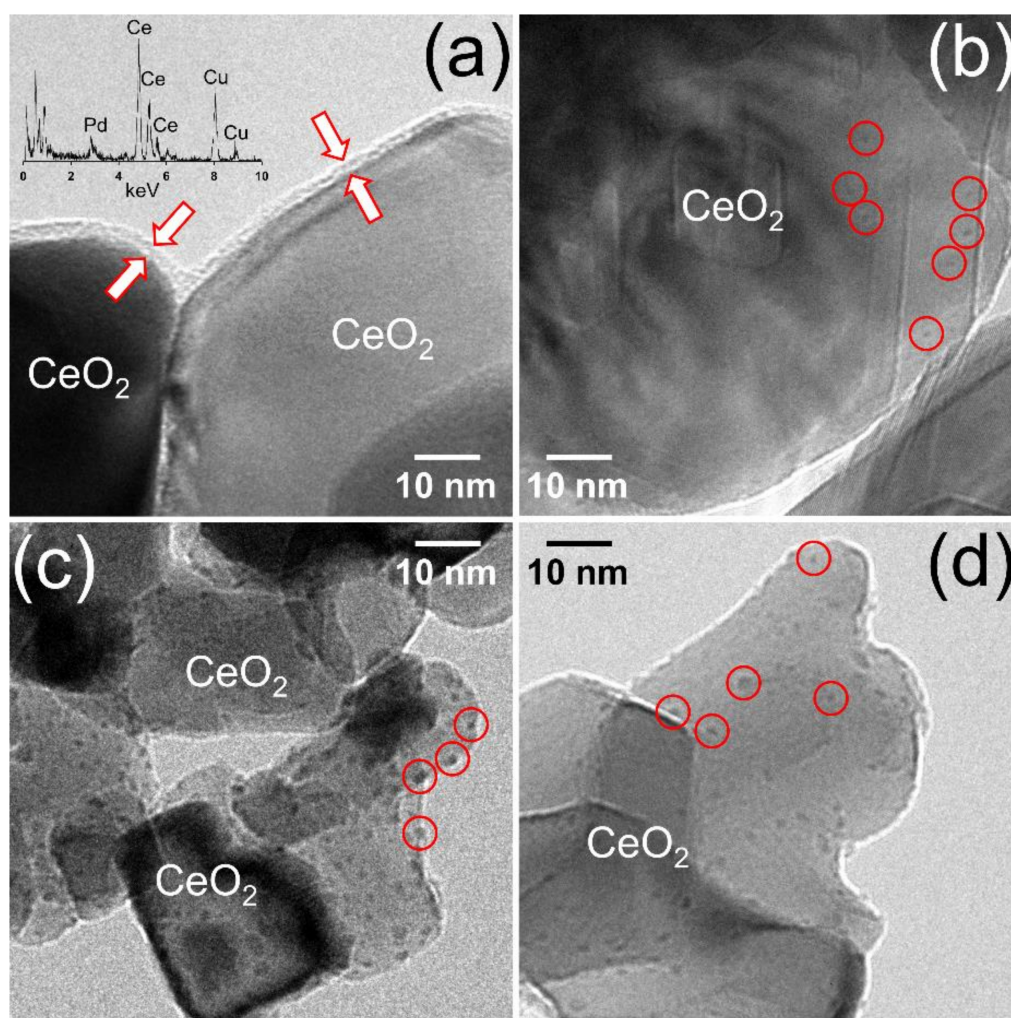


Figure 1. HRTEM images of the Pd/ CeO_2 catalysts prepared by milling CeO_2 and Pd acetate (a) or Pd nitrate (b) at 50 Hz for 10 min, and catalysts prepared by incipient wetness impregnation with Pd acetate (c) or Pd nitrate (d). All catalysts contain a nominal Pd loading of 1 wt.%.

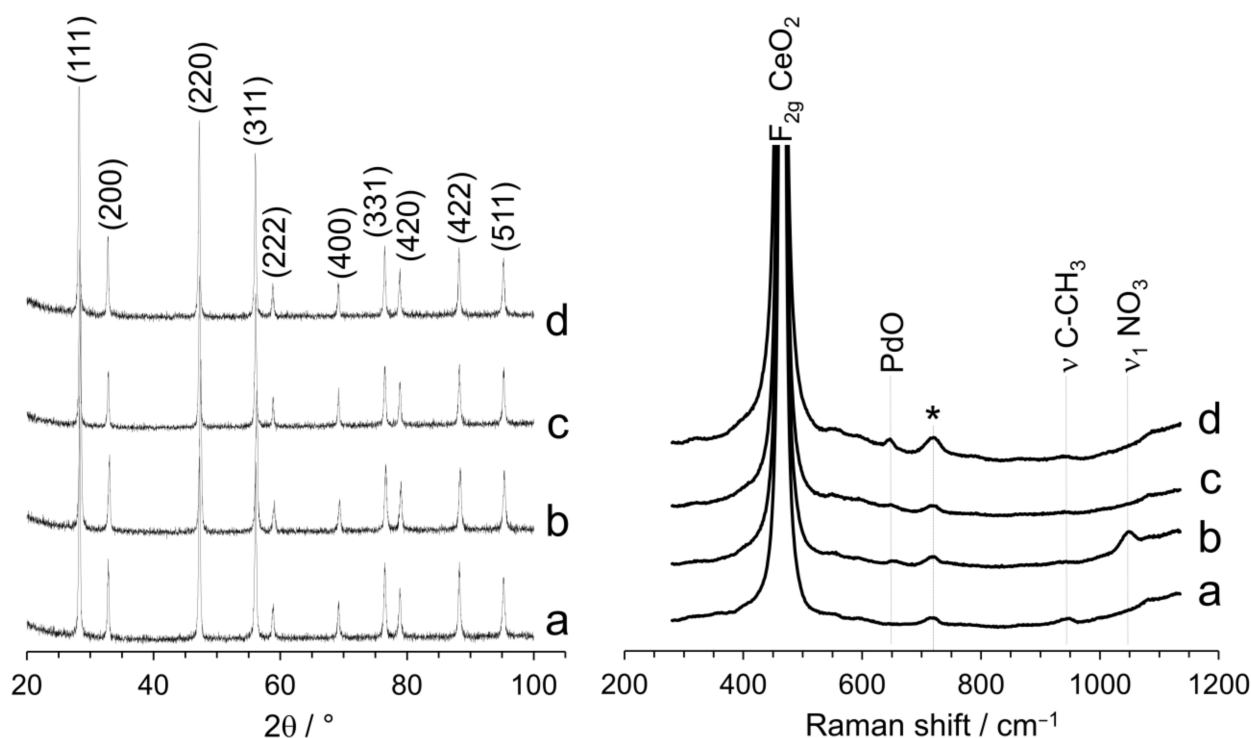


Figure 2. XRD profiles and Raman spectra of Pd/CeO₂ catalysts prepared by milling CeO₂ and Pd acetate (a) or Pd nitrate (b) at 50 Hz for 10 min, and catalysts prepared by incipient wetness impregnation with Pd acetate (c) or Pd nitrate (d). All catalysts contain a nominal Pd loading of 1 wt.%.

The surface of the catalysts was analyzed by X-ray photoelectron spectroscopy (XPS). Figure 3 shows the Pd 3d XP spectra of the catalysts studied by HRTEM, XRD and Raman spectroscopy discussed above. There are important differences among the XP spectra, in particular between the samples prepared by mechanochemical methods and those prepared by conventional impregnation. The Pd 3d spectra of the samples prepared by impregnation showed exactly the same pattern, independently of the Pd precursor used (Figure 3c,d). The Pd 3d_{5/2} spectra contain two bands at about 336.4 and 338.0 eV, which correspond well to Pd²⁺ and Pd⁴⁺ species, respectively [21,24]. The surface atomic ratio Pd⁴⁺/(Pd⁴⁺+Pd²⁺) in these samples prepared by impregnation is about 0.2. In contrast, the spectra of the samples prepared by ball milling were quite different. The sample prepared by milling ceria and Pd nitrate (Figure 3b) exhibited a unique band at 337.7 eV, whereas the spectrum of the sample prepared by milling ceria and Pd acetate (Figure 3a) exhibited two bands at 336.0 and 337.6 eV, which represent a shift of 0.4 eV to lower energy values with respect to the samples prepared by impregnation. These differences demonstrate that the electronic state of palladium at the surface of the catalysts strongly depends on the preparation method. The shift to lower binding energy values in the samples prepared by mechanochemistry is indicative of surface oxidized Pd strongly interacting with ceria [30–32], which is in agreement with HRTEM and Raman spectroscopy data. In addition, the surface atomic ratio Pd⁴⁺/(Pd⁴⁺+Pd²⁺) is much higher in the samples prepared by mechanochemistry and the values depend on the Pd precursor used; for the sample prepared by milling ceria and Pd acetate, this value is 0.6, which is much higher than the value recorded in the catalyst prepared by impregnation with Pd acetate (0.2). Therefore, it is concluded that Pd⁴⁺ species strongly interacting with ceria are easily accommodated on the surface of catalysts prepared by mechanochemical methods. On the other hand, XPS yields also valuable information about the dispersion of Pd. The surface atomic ratio Pd/(Pd+Ce) is higher in the sample prepared by milling ceria and Pd acetate with respect to the sample prepared by milling ceria and Pd nitrate (0.29 and 0.14, respectively) and to the samples

prepared by impregnation (about 0.2). The high Pd dispersion measured by XPS for the sample prepared by milling ceria and Pd acetate is in accordance with the existence of the amorphous shell identified by HRTEM (Figure 1a).

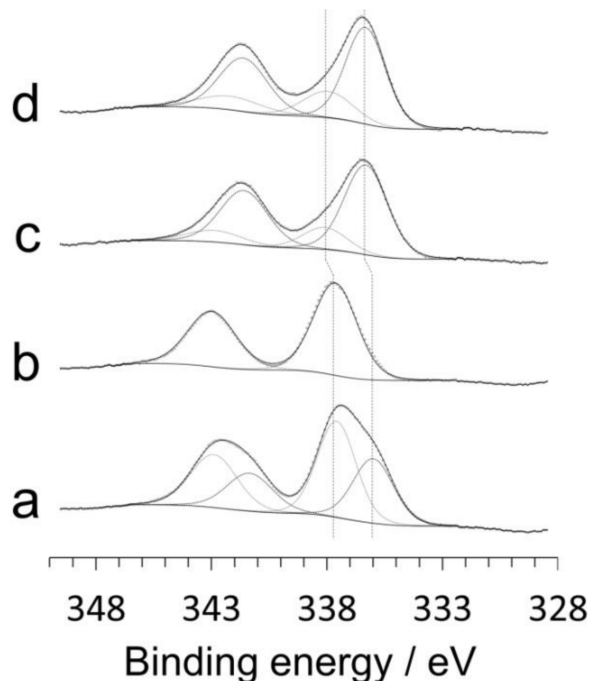


Figure 3. Pd 3d X-ray photoelectron spectra of the Pd/CeO₂ catalysts prepared by milling CeO₂ and Pd acetate (a) or Pd nitrate (b) at 50 Hz for 10 min, and catalysts prepared by incipient wetness impregnation with Pd acetate (c) or Pd nitrate (d). All catalysts contain a nominal Pd loading of 1 wt.%.

3.2. Catalytic Tests

Temperature-dependent catalytic measurements were carried out between 200 and 600 °C at GHSV = $12 \times 10^3 \text{ h}^{-1}$, CH₄:air:N₂ = 4:11:85 (molar basis) and F/W = 60 L h⁻¹ g⁻¹. In all cases, the profiles of the disappearance of reactants (methane and oxygen) and the appearance of products (syngas and carbon dioxide) at different reaction temperatures followed similar patterns. As a representative example, Figure 4a shows these profiles recorded over the Pd/CeO₂ (0.5 wt.% Pd) catalyst prepared by milling palladium acetate and CeO₂ at 50 Hz for 5 min. As expected, the conversion of methane progressively increased with temperature, whereas oxygen was rapidly consumed at low temperatures (≤ 350 °C). The consumption of oxygen was accompanied by the simultaneous appearance of H₂O and CO₂ in a H₂O:CO₂ ratio of about 2:1 (molar basis). Additionally, in the range 200–350 °C, the consumption of oxygen doubled that of methane, and the amount of CO₂ formed equaled the amount of methane consumed. Overall, this distribution of species clearly indicates that the direct combustion of methane takes place in this temperature range, $\text{CH}_4 + 2\text{O}_2 \rightarrow \text{CO}_2 + 2\text{H}_2\text{O}$. At 400 °C, when all the oxygen was consumed, the consumption of methane was accompanied by the simultaneous consumption of H₂O, being the amount of water consumed double than that of methane. At the same time, CO₂ and hydrogen were produced. The amount of CO₂ produced equaled the amount of methane consumed, and the amount of hydrogen produced was about four times that of methane consumed. This distribution of species corresponds well to the methane steam reforming reaction, $\text{CH}_4 + \text{H}_2\text{O} \rightleftharpoons \text{CO} + 3\text{H}_2$. At temperatures ≥ 450 °C, the transformation of methane was accompanied by the progressive consumption of not only H₂O, but also CO₂. At the same time, the production of syngas (H₂ and CO) was boosted, which was pro-

duced by the simultaneous occurrence of the steam reforming and dry reforming reactions of methane, $\text{CH}_4 + \text{H}_2\text{O} \rightleftharpoons \text{CO} + 3\text{H}_2$ and $\text{CH}_4 + \text{CO}_2 \rightleftharpoons 2\text{CO} + 2\text{H}_2$, respectively. This reaction mechanism corresponds well with the so-called “combustion and reforming reaction (CRR)” mechanism for POM [7,8]. For comparison, Figure 4b shows the distribution of products obtained at different temperatures with the Pd/CeO₂ (0.5 wt.% Pd) catalyst prepared with Pd acetate by incipient wetness impregnation. Similar trends were observed in the disappearance of reactants and the appearance of products, which indicates that the reaction mechanism is the same as that discussed above, but the temperatures at which the different processes took place shifted to higher values, about 100 °C, indicating lower catalytic activity.

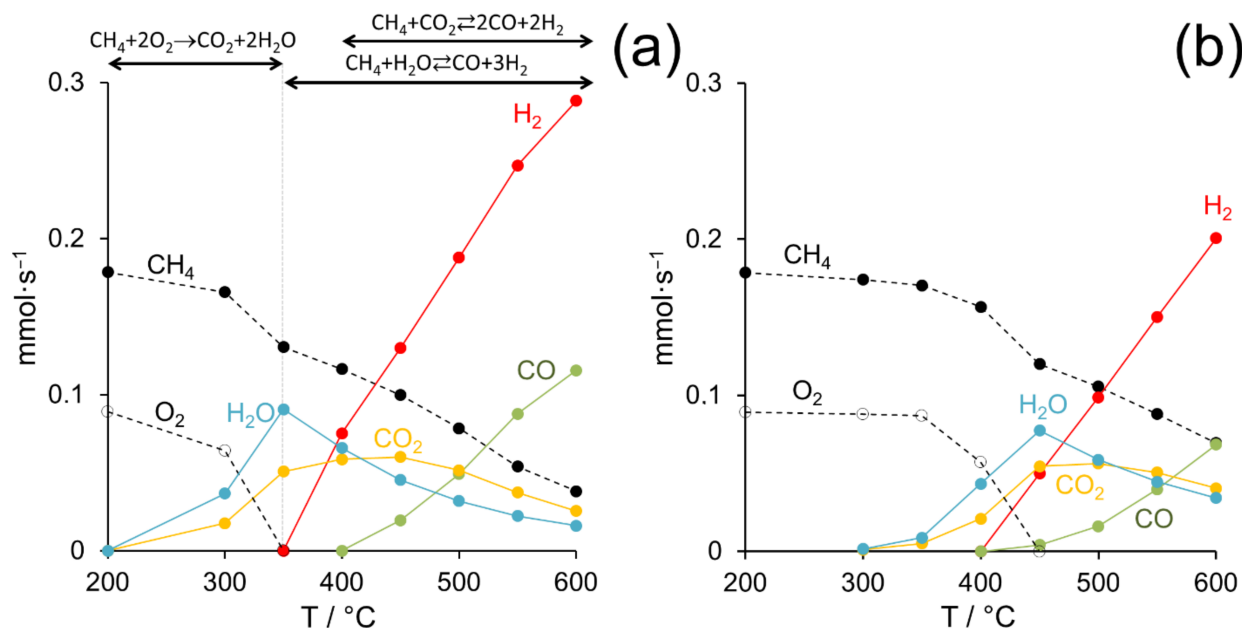


Figure 4. Molar flows of the different species present during the partial oxidation of methane on Pd/CeO₂ (0.5 wt.% Pd) prepared by dry ball milling from palladium acetate and CeO₂ at 50 Hz for 5 min (a) and by incipient wetness impregnation of CeO₂ with Pd acetate (b). GHSV = $12 \times 10^3 \text{ h}^{-1}$, F/W = $60 \text{ L h}^{-1} \text{ g}^{-1}$.

Taking into account the two consecutive steps involved in the POM mechanism on Pd/CeO₂ catalysts, from now on only the results obtained at temperatures above 450 °C will be considered, since below this temperature, the production of syngas is not significant. Table 1 compiles the results obtained for all catalysts tested in terms of methane conversion and hydrogen selectivity at 450 and 550 °C, and CO selectivity at 550 °C. The results obtained on bare ceria as prepared and after milling at 50 Hz for 10 min are also included as blank runs. The ceria support is totally inactive for POM under the reaction conditions tested, and ball milling ceria in the absence of Pd does not result in any reactivity.

The catalytic performances of the catalysts prepared by dry ball milling demonstrate that the Pd salt used as precursor has a strong influence on catalytic activity. Figure 5 corresponds to data selected from Table 1 to perform accurate comparisons between different catalysts. In Figure 5a, the effect of milling time for samples containing 1 wt.% Pd and prepared at 50 Hz with Pd nitrate or Pd acetate precursors is shown. Clearly, at short milling times (5 and 10 min) the activity of samples prepared with Pd acetate outperforms those of samples prepared with Pd nitrate, whereas after long milling time (20 min) the methane conversion on both samples became similar. Interestingly, the longer the milling time, the higher the activity of the catalysts prepared with Pd nitrate. This suggests that a particular and delicate Pd-CeO₂ architecture is formed at a short milling time using Pd acetate, which is highly active for POM. Contrarily, if a long milling time is used, the resulting metal-support interaction is independent of the Pd salt used as a

precursor. This could be attributed to the peculiar decomposition of Pd acetate, which first decomposes to metallic Pd and then gradually oxidizes to PdO in contrast to Pd nitrate, which decomposes directly to PdO [33]. Recently, it has been claimed that for Pd/CeO₂ systems, a metal-core-oxide-shell structure is responsible for a high activity for methane combustion [34]. The different decomposition pathways of Pd acetate and Pd nitrate would likely result in different Pd-ceria interactions developed during the POM reaction. These observations are also supported by Figure 5b, where the effect of the energy of ball milling (frequency) is shown for the samples containing 1 wt.% Pd after 10 min. It is deduced that high-energy milling has a beneficial effect on catalytic activity for the samples prepared with Pd acetate, which suggests that a strong Pd-CeO₂ interaction favors the activation of the methane molecule, whereas an opposite trend is observed in samples prepared with Pd nitrate. On the other hand, two ball-milled samples (50 Hz and 10 min) prepared with Pd acetate and Pd nitrate and calcined at 300 °C to remove the acetate and nitrate groups, respectively, yielded different results (Table 1). Whereas the catalytic activity of the ball milled sample prepared with Pd acetate decreased slightly after calcination, the sample prepared with Pd nitrate showed a clear improvement after the calcination treatment, which suggests that the presence of nitrate residues on the catalyst surface is detrimental for the reaction.

Table 1. Methane conversion and selectivity of hydrogen and carbon monoxide obtained at 450 and 550 °C on bare ceria, ceria after ball milling, and Pd/CeO₂ catalysts prepared by incipient wetness impregnation (IWI) and dry ball milling (BM) using different synthesis parameters and metal loading values.

	Pd Precursor	Hz	min	wt.% Pd	$x_{CH_4}^{450\text{ }^\circ\text{C}}$	$x_{CH_4}^{550\text{ }^\circ\text{C}}$	$S_{H_2}^{450\text{ }^\circ\text{C}}$	$S_{H_2}^{550\text{ }^\circ\text{C}}$	$S_{CO}^{550\text{ }^\circ\text{C}}$
	CeO ₂	0	0	0	0	0	0	0	0
		50	10	0	0	0	0	0	0
BM	acetate	15	10	1	34.9	47.0	54.8	92.9	49.2
		30	10	1	35.5	55.9	53.4	88.3	52.0
		50	5	1	42.5	70.2	71.1	95.8	66.4
		50	10	1	38.9	64.1	63.5	89.9	57.8
		50	10	1 ^a	33.5	55.8	56.5	93.1	56.2
		50	20	1	36.8	58.5	56.8	88.8	53.4
		50	5	0.5	44.1	69.7	82.0	98.8	70.3
		50	5	2	39.7	67.5	73.1	98.3	68.1
BM	nitrate	15	10	1	35.2	54.9	47.9	84.8	48.2
		30	10	1	31.5	51.0	61.7	96.1	54.6
		50	5	1	30.7	47.0	58.3	92.9	49.2
		50	10	1	30.5	53.2	67.1	99.8	60.0
		50	10	1 ^a	45.4	70.2	84.8	99.9	75.2
		50	20	1	32.7	55.7	68.6	99.8	62.7
		50	10	0.5	32.6	52.7	48.2	86.7	48.6
		50	10	2	39.9	66.8	64.1	94.0	63.9
IWI	acetate	0	0	0.5	32.8	50.7	42.4	82.6	43.8
		0	0	1	35.9	59.2	51.6	89.0	54.8
		0	0	2	37.0	62.3	57.2	91.8	58.0
		50	5 ^b	1	34.2	57.0	57.0	92.7	56.5
IWI	nitrate	0	0	0.5	39.7	67.7	72.8	98.3	68.4
		0	0	1	34.5	57.4	55.8	90.9	54.6
		0	0	2	32.8	56.0	61.3	99.1	62.1
		50	10 ^b	1	34.8	59.2	61.9	95.1	59.5

^a calcined at 300 °C for 1 h; ^b impregnation on previously ball-milled CeO₂

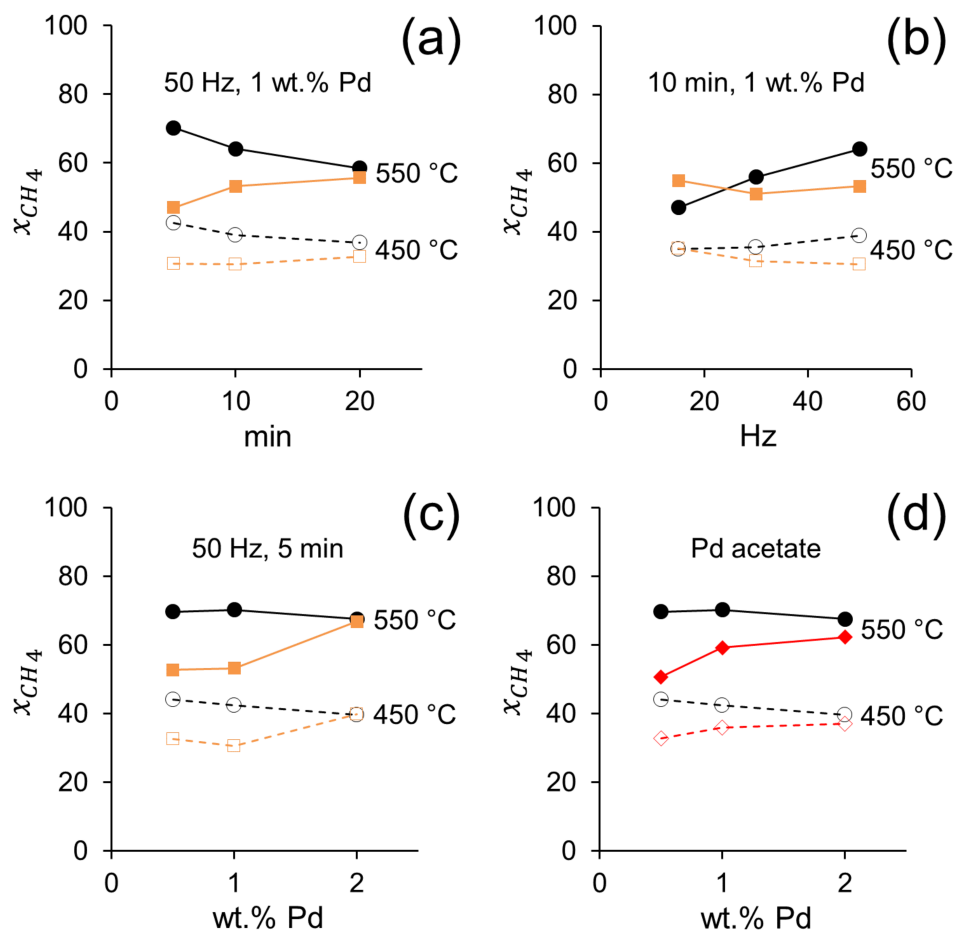


Figure 5. Conversion of methane at 450 and 550 °C on Pd/CeO₂ catalysts prepared by milling CeO₂ and palladium acetate (black) or palladium nitrate (orange) at different milling time (a), frequency (b) and Pd loading (c). Conversion of methane on Pd/CeO₂ prepared by milling CeO₂ and palladium acetate for 5 min at 50 Hz (black) and by incipient wetness impregnation of palladium acetate (red) (d). GHSV = $12 \times 10^3 \text{ h}^{-1}$, F/W = $60 \text{ L h}^{-1} \text{ g}^{-1}$.

Recent density functional theory (DFT) calculations have shown that Pd_xCe_{1-x}O_δ surfaces are particularly effective in the activation of the C-H bonds in the methane molecule [33,35], and that substitution of Ce by Pd ions originates highly active and stable systems [36,37]. The mechanochemical forces that operate in the ball milling preparation method would enhance the formation of such active surfaces and substituted structures, as demonstrated recently in the total oxidation of methane [21]. In fact, the amorphous shell observed in the HRTEM images of the Pd/CeO₂ catalyst prepared by ball milling ceria and Pd acetate (Figure 1) is expected to be particularly active due to undercoordinated sites, as claimed recently by DFT calculations for the activation of methane [38]. Important information is obtained from Figure 5c, where the methane conversion is plotted against the Pd loading for samples ball milled at 50 Hz for 5 min. For the catalysts prepared with Pd nitrate, the higher the Pd content the higher the methane conversion. In contrast, the opposite trend is true for the catalysts prepared with Pd acetate, which is in accordance with the assumption that low Pd contents are required to build up active Pd_xCe_{1-x}O_δ surfaces, whereas high Pd loadings result in the accumulation of other less active Pd species on the surface. Finally, Figure 5d clearly shows that the catalytic performances of the Pd/CeO₂ catalysts prepared by incipient wetness impregnation from Pd acetate are less active than the catalysts prepared by ball milling with Pd acetate for any Pd loading. Indeed, the performances of the catalysts prepared by ball milling with Pd nitrate are similar to those

exhibited by Pd/CeO₂ catalysts prepared by conventional incipient wetness impregnation, again pointing out to an extraordinary catalytic behavior induced by the amorphous Pd_xCe_{1-x}O_δ surface in the catalysts prepared by ball milling with Pd acetate. Finally, to investigate if the better catalytic performance of the ball milled samples is due to defects and/or structural changes of the ceria support induced by the mechanochemical method, we tested IWI samples prepared with previously ball milled CeO₂ using exactly the same conditions. The catalytic performance of the IWI samples using fresh CeO₂ and previously milled CeO₂ are virtually identical (Table 1), which means that the catalytic behavior of the Pd/CeO₂ samples prepared by ball milling is not related to the ceria support, but to a specific interaction between CeO₂ and Pd induced by the mechanochemical method.

A stability test was carried out for more than 100 h at 550 °C on the sample prepared by milling CeO₂ and Pd acetate for 5 min at 50 Hz with a Pd loading of 0.5 wt.%, since this sample exhibited good methane conversion and selectivity to syngas (see Table 1), and, for comparative purposes, on the sample prepared by incipient wetness impregnation with Pd acetate (0.5 wt.% Pd). Figure 6a shows the methane conversion for both catalysts. A slight deactivation of the sample prepared by mechanochemical methods is observed, especially during the first 50 h of operation, where the methane conversion rate decreased by approximately 0.15 % h⁻¹. After 50 h, the deactivation decreased by only 0.04 % h⁻¹, the methane conversion stabilized at about 63 % and the selectivity to H₂ and CO was ca. 94 and 58 %, respectively. In contrast, the conventional sample prepared by impregnation deactivated more severely; during the first 50 h of operation the methane conversion rate decreased significantly by 0.48 % h⁻¹ and after 50 h of reaction the methane conversion rate still decreased by 0.23 % h⁻¹ and did not stabilize. Since the dry reforming of methane is involved in the reaction mechanism and generally causes carbon deposition on the catalyst, we recorded the Raman spectra in the carbon region for the two samples after reaction (Figure 6b). The Raman spectrum of the sample after the reaction prepared by milling ceria and Pd acetate showed a broad signal at approximately 1180 cm⁻¹, which corresponds to the second-order longitudinal optical mode (2LO) of CeO₂ [25]. In contrast, the Raman spectrum of the sample after the reaction prepared by impregnation showed, in addition to the signal at ca. 1180 cm⁻¹ due to CeO₂, the characteristic D and G bands of carbon at approximately 1340 and 1580 cm⁻¹, respectively. Even if the intensity of the carbon bands is certainly low, the occurrence of carbon deposition may explain the deactivation observed for this sample. Therefore, the sample prepared by mechanical forces is not only more active, but remarkably more stable under reaction. This robustness makes this catalyst a good candidate for practical application. In addition, it contains a low metal loading.

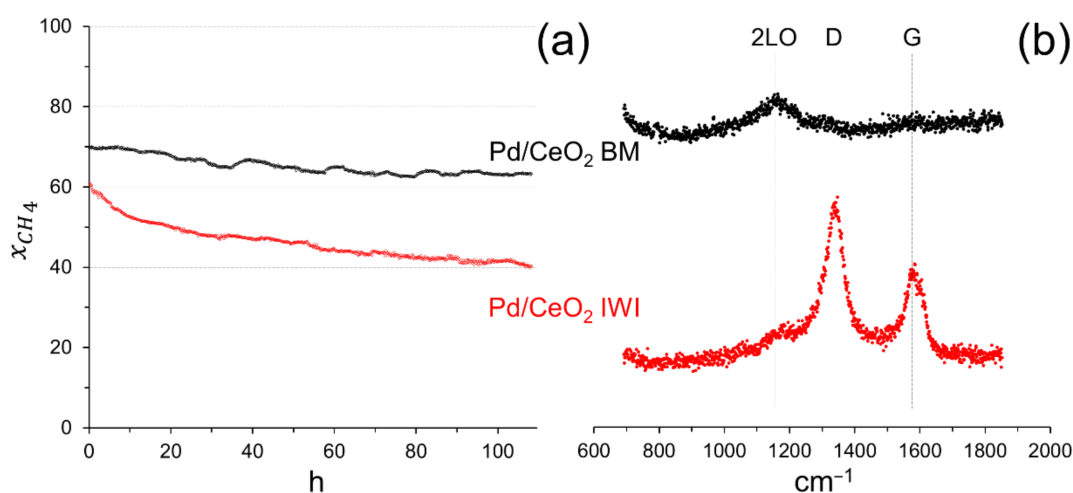


Figure 6. (a) Methane conversion in a long-term stability test at 550 °C on Pd/CeO₂ prepared by milling CeO₂ and Pd acetate (5 min at 50 Hz, 0.5 wt.% Pd; Pd/CeO₂ BM) and by incipient wetness impregnation with Pd acetate (Pd/CeO₂ IWI). GHSV = 12×10^3 h⁻¹, F/W = 60 L h⁻¹ g⁻¹. (b) Raman spectra recorded on the samples after reaction.

4. Conclusions

A series of Pd/CeO₂ catalysts were prepared, characterized with HRTEM, XRD, Raman spectroscopy and XPS, and tested for the partial oxidation of methane at low temperature to obtain syngas. Two different preparation methods were used to synthesize the catalysts, conventional incipient wetness impregnation and dry ball milling. Two metal precursors were used, palladium nitrate and palladium acetate, and the metal loading was varied from 0.5 to 2 wt.% Pd. For the ball-milled samples, the influence of milling energy (5–50 Hz) and milling time (5–20 min) on catalytic performance has been evaluated. Catalysts prepared by mechanochemistry using Pd acetate have shown better catalytic performance than catalysts prepared by mechanochemistry using Pd nitrate and catalysts prepared by incipient wetness impregnation, either with Pd acetate or with Pd nitrate. The best catalytic performance has been obtained with a catalyst prepared by milling ceria and Pd acetate for 5 min at 50 Hz with a metal loading of 0.5 % by weight of palladium, which has also shown good catalytic stability in a 100 h experiment duration. Catalysts prepared by incipient wetness impregnation contain well-defined PdO nanoparticles. In contrast, catalysts prepared by milling ceria and Pd acetate contain a unique Pd-CeO₂ architecture characterized by a 2–3 nm thick amorphous layer with highly oxidized Pd (Pd⁴⁺-like) on the surface that strongly interacts with ceria, which is very active for methane partial oxidation. These results encourage the use of mechanochemistry as an easy, clean and efficient way to prepare active metal supported catalysts for the partial oxidation of methane to obtain syngas. Future work will focus on the use of mechanochemistry to prepare other formulations involving different metals and supports, as well as bimetallic systems.

Author Contributions: Conceptualization, J.L. and X.V.; Funding acquisition, J.L.; Investigation, S.F.; Supervision, X.V. and J.L.; Writing: original draft, J.L.; Writing: review & editing, X.V. and S.F. All authors have read and agreed to the published version of the manuscript.

Funding: This research was funded by MICINN/FEDER grant number RTI2018-093996-B-C31 and by Generalitat de Catalunya grant number 2017 SGR 128.

Acknowledgments: S.F. is grateful to Generalitat de Catalunya for PhD grant 2019 FI_B 00908. X.V. is grateful to Spanish Government, Ministerio de Ciencia, Innovación y Universidades Juan de la Cierva-Incorporación program for an individual fellowship grant agreement IJCI-2017-31449. J.L. is a Serra Hünter Fellow and is grateful to ICREA Academia program.

Conflicts of Interest: The authors declare no conflict of interest.

References

1. Lunsford, J.H. Catalytic conversion of methane to more useful chemicals and fuels: A challenge for the 21st century. *Catal. Today* **2000**, *63*, 165–174. [[CrossRef](#)]
2. Rostrup-Nielsen, T. Manufacture of hydrogen. *Catal. Today* **2005**, *106*, 293–296. [[CrossRef](#)]
3. Navarro, R.M.; Peña, A.M.A.; Fierro, J.L.G. Hydrogen Production Reactions from Carbon Feedstocks: Fossil Fuels and Biomass. *Chem. Rev.* **2007**, *107*, 3952–3991. [[CrossRef](#)] [[PubMed](#)]
4. Sokolovskii, V.; Coville, N.; Parmaliana, A.; Eskendirov, I.; Makoa, M. Methane partial oxidation. Challenge and perspective. *Catal. Today* **1998**, *42*, 191–195. [[CrossRef](#)]
5. Chen, L.; Qi, Z.; Zhang, S.; Su, J.; Somorjai, G.A. Catalytic Hydrogen Production from Methane: A Review on Recent Progress and Prospect. *Catalysis* **2020**, *10*, 858. [[CrossRef](#)]
6. Ma, R.; Xu, B.; Zhang, X. Catalytic partial oxidation (CPOX) of natural gas and renewable hydrocarbons/oxygenated hydrocarbons—A review. *Catal. Today* **2019**, *338*, 18–30. [[CrossRef](#)]
7. Enger, C.B.; Lødeng, R.; Holmen, A. A review of catalytic partial oxidation of methane to synthesis gas with emphasis on reaction mechanisms over transition metal catalysts. *Appl. Catal. A Gen.* **2008**, *346*, 1–27. [[CrossRef](#)]
8. York, A.P.E.; Xiao, T.; Green, M.L.H. Brief Overview of the Partial Oxidation of Methane to Synthesis Gas. *Top. Catal.* **2003**, *22*, 345–358. [[CrossRef](#)]
9. Freni, S.; Calogero, G.; Cavallaro, S. Hydrogen production from methane through catalytic partial oxidation reactions. *J. Power Sources* **2000**, *87*, 28–38. [[CrossRef](#)]
10. Slagtern, A.; Swaan, H.M.; Olsbye, U.; Dahl, I.M.; Mirodatos, C. Catalytic partial oxidation of methane over Ni-, Co- and Fe-based catalysts. *Catal. Today* **1998**, *46*, 107–115. [[CrossRef](#)]

11. Ashcroft, A.T.; Cheetham, A.K.; Foord, J.S.; Green, M.L.H.; Grey, C.P.; Murrell, A.J.; Vernon, P.D.F. Selective oxidation of methane to synthesis gas using transition metal catalysts. *Nat. Cell Biol.* **1990**, *344*, 319–321. [[CrossRef](#)]
12. Hickman, D.A.; Schmidt, L.D. Production of Syngas by Direct Catalytic Oxidation of Methane. *Science* **1993**, *259*, 343–346. [[CrossRef](#)] [[PubMed](#)]
13. Zhu, Y.; Zhang, S.; Shan, J.-J.; Nguyen, L.; Zhan, S.; Gu, X.; Tao, F. In Situ Surface Chemistries and Catalytic Performances of Ceria Doped with Palladium, Platinum, and Rhodium in Methane Partial Oxidation for the Production of Syngas. *ACS Catal.* **2013**, *3*, 2627–2639. [[CrossRef](#)]
14. Moral, A.; Reyero, I.; Llorca, J.; Bimbela, F.; Gandía, L. Partial oxidation of methane to syngas using Co/Mg and Co/Mg-Al oxide supported catalysts. *Catal. Today* **2019**, *333*, 259–267. [[CrossRef](#)]
15. Osman, A.I. Catalytic Hydrogen Production from Methane Partial Oxidation: Mechanism and Kinetic Study. *Chem. Eng. Technol.* **2020**, *43*, 641–648. [[CrossRef](#)]
16. Toso, A.; Colussi, S.; Llorca, J.; Trovarelli, A. The dynamics of PdO-Pd phase transformation in the presence of water over Si-doped Pd/CeO₂ methane oxidation catalysts. *Appl. Catal. A Gen.* **2019**, *574*, 79–86. [[CrossRef](#)]
17. Soler, L.; Casanovas, A.; Escudero, C.; Perez-Dieste, V.; Aneghi, E.; Trovarelli, A.; Llorca, J. Ambient pressure photoemission spectroscopy reveals the mechanism of carbon soot oxidation in ceria-based catalysts. *ChemCatChem* **2016**, *8*, 2748–2751.
18. Aneghi, E.; Llorca, J.; Trovarelli, A.; Aouine, M.; Vernoux, P. In situ environmental HRTEM discloses low temperature carbon soot oxidation by ceria-zirconia at the nanoscale. *Chem. Commun.* **2019**, *55*, 3876–3878. [[CrossRef](#)]
19. Aneghi, E.; Rico-Perez, V.; De Leitenburg, C.; Maschio, S.; Soler, L.; Llorca, J.; Trovarelli, A. Ceria-Zirconia Particles Wrapped in a 2D Carbon Envelope: Improved Low-Temperature Oxygen Transfer and Oxidation Activity. *Angew. Chem. Int. Ed.* **2015**, *54*, 14040–14043. [[CrossRef](#)] [[PubMed](#)]
20. Colussi, S.; Gayen, A.; Camellone, M.F.; Boaro, M.; Llorca, J.; Fabris, S.; Trovarelli, A. Nanofaceted Pd-O Sites in Pd-Ce Surface Superstructures: Enhanced Activity in Catalytic Combustion of Methane. *Angew. Chem. Int. Ed.* **2009**, *48*, 8481–8484. [[CrossRef](#)] [[PubMed](#)]
21. Danielis, M.; Colussi, S.; De Leitenburg, C.; Soler, L.; Llorca, J.; Trovarelli, A. Outstanding Methane Oxidation Performance of Palladium-Embedded Ceria Catalysts Prepared by a One-Step Dry Ball-Milling Method. *Angew. Chem.* **2018**, *130*, 10369–10373. [[CrossRef](#)]
22. Danielis, M.; Colussi, S.; De Leitenburg, C.; Soler, L.; Llorca, J.; Trovarelli, A. The effect of milling parameters on the mechanochemical synthesis of Pd–CeO₂ methane oxidation catalysts. *Catal. Sci. Technol.* **2019**, *9*, 4232–4238. [[CrossRef](#)]
23. Adjianto, L.; Bennett, D.A.; Chen, C.; Yu, A.S. Exceptional thermal stability of Pd@CeO₂ core-shell catalyst nanostructures grafted onto an oxide surface. *Nano Lett.* **2013**, *13*, 2252–2257. [[CrossRef](#)] [[PubMed](#)]
24. Danielis, M.; Betancourt, L.E.; Orozco, I.; Divins, N.J.; Llorca, J.; Rodríguez, J.A.; Senanayake, S.D.; Colussi, S.; Trovarelli, A. Methane oxidation activity and nanoscale characterization of Pd/CeO₂ catalysts prepared by dry milling Pd acetate and ceria. *Appl. Catal. B Environ.* **2021**, *282*, 119567. [[CrossRef](#)]
25. Wu, Z.; Li, M.; Howe, J.; Meyer, I.H.M.; Overbury, S.H. Probing Defect Sites on CeO₂ Nanocrystals with Well-Defined Surface Planes by Raman Spectroscopy and O₂ Adsorption. *Langmuir* **2010**, *26*, 16595–16606. [[CrossRef](#)] [[PubMed](#)]
26. Weber, W.; Hass, K.; McBride, J. Raman study of CeO₂: Second-order scattering, lattice dynamics, and particle-size effects. *Phys. Rev. B* **1993**, *48*, 178. [[CrossRef](#)]
27. Kosacki, I.; Suzuki, T.; Anderson, H.U.; Colomban, P. Raman scattering and lattice defects in nanocrystalline CeO₂ thin films. *Solid State Ion.* **2002**, *149*, 99–105. [[CrossRef](#)]
28. Waterland, M.R.; Stockwell, D.; Kelley, A.M. Symmetry breaking effects in NO₃⁻: Raman spectra of nitrate salts and ab initio resonance Raman spectra of nitrate–water complexes. *J. Chem. Phys.* **2001**, *114*, 6249–6258. [[CrossRef](#)]
29. Ma, J.; Lou, Y.; Cai, Y.; Zhao, Z.; Wang, L.; Zhan, W.; Guo, Y.; Guo, Y. The relationship between the chemical state of Pd species and the catalytic activity for methane combustion on Pd/CeO₂. *Catal. Sci. Technol.* **2018**, *8*, 2567–2577. [[CrossRef](#)]
30. Slavinskaya, E.M.; Stonkus, O.A.; Guliaev, R.V.; Lapin, I.N.; Svetlichnyi, V.A.; Boronin, A.I.; Kardash, T.Y. Metal–support interaction in Pd/CeO₂ model catalysts for CO oxidation: From pulsed laser-ablated nanoparticles to highly active state of the catalyst. *Catal. Sci. Technol.* **2016**, *6*, 6650–6666. [[CrossRef](#)]
31. Divins, N.J.; Angurell, I.; Escudero, C.; Pérez-Dieste, V.; Llorca, J. Influence of the support on surface rearrangements of bimetallic nanoparticles in real catalysts. *Science* **2014**, *346*, 620–623. [[CrossRef](#)] [[PubMed](#)]
32. Garcia, X.; Soler, L.; Divins, N.J.; Vendrell, X.; Serrano, I.; Lucentini, I.; Prat, J.; Solano, E.; Tallarida, M.; Escudero, C.; et al. Ceria-Based Catalysts Studied by Near Ambient Pressure X-ray Photoelectron Spectroscopy: A Review. *Catalysis* **2020**, *10*, 286. [[CrossRef](#)]
33. Senftle, T.P.; Van Duin, A.C.T.; Janik, M.J. Methane Activation at the Pd/CeO₂ Interface. *ACS Catal.* **2016**, *7*, 327–332. [[CrossRef](#)]
34. Murata, K.; Kosuge, D.; Ohyama, J.; Mahara, Y.; Yamamoto, Y.; Arai, S.; Satsuma, A. Exploiting Metal–Support Interactions to Tune the Redox Properties of Supported Pd Catalysts for Methane Combustion. *ACS Catal.* **2019**, *10*, 1381–1387. [[CrossRef](#)]
35. Senftle, T.P.; van Duin, A.C.; Janik, M.J. Role of Site Stability in Methane Activation on Pd_xCe_{1-x}O_δ Surfaces. *ACS Catalysis* **2015**, *5*, 6187–6199. [[CrossRef](#)]
36. Su, Y.-Q.; Filot, I.A.W.; Liu, J.-X.; Hensen, E.J.M. Stable Pd-Doped Ceria Structures for CH₄ Activation and CO Oxidation. *ACS Catal.* **2018**, *8*, 75–80. [[CrossRef](#)]

-
37. Su, Y.-Q.; Liu, J.-X.; Filot, I.A.W.; Zhang, L.; Hensen, E.J.M. Highly Active and Stable CH₄ Oxidation by Substitution of Ce⁴⁺ by Two Pd²⁺ Ions in CeO₂(111). *ACS Catal.* **2018**, *8*, 6552–6559. [[CrossRef](#)]
 38. Bunting, R.J.; Cheng, X.; Thompson, J.M.; Hu, P. Amorphous Surface PdO_x and Its Activity toward Methane Combustion. *ACS Catal.* **2019**, *9*, 10317–10323. [[CrossRef](#)]